Characterization of stacking faults in thick 3C-SiC crystals using high-resolution diffuse X-ray scattering

Alexandre Boulle, D. Chaussende, F. Conchon, G. Ferro, O. Masson

Characterization of stacking faults in thick 3C-SiC crystals using high-resolution diffuse X-ray scattering

A. Boulle [1], D. Chaussende [2], F. Conchon [1], G. Ferro [3], O. Masson [1]

[1] Science des Procédés Céramiques et de Traitements de Surface CNRS UMR 6638, ENSCI 47 avenue Albert Thomas 87065 Limoges Cedex, France

[2] Laboratoire des Matériaux et du Génie Physique CNRS UMR 5628, Minatec INPGrenoble, 3 parvis Louis Néel, BP 257, 38016 Grenoble Cedex 01, France

[3] Laboratoire des Multimatériaux et Interfaces CNRS UMR 5615, 43 boulevard du 11 novembre 1918, 69622 Villeurbanne Cedex, France

Abstract

A novel non-destructive method to characterize stacking faults (SF) in 3C-SiC crystals is presented. This method is based on fast X-ray diffraction reciprocal space mapping and can be used qualitatively for routine analysis of 3C-SiC as SFs give rise to a characteristic star-like pattern in reciprocal space whose intensity depends on the SF density. The simulation of the diffusely scattered intensity streaks with an appropriate model enables one to also obtain quantitative results such as SF densities, mosaic domain size and mosaicity. The model is tested with a commercial (001) 3C-SiC crystal from HAST corporation, and then it is used to analyse SFs in (111) 3C-SiC crystals grown by continuous feed – physical vapour transport.

1. Introduction

Among the more than 200 SiC polytypes, the cubic silicon carbide (3C-SiC) exhibits the highest electron mobility and isotropic electrical properties which make it the most desirable polytype for active device applications [1]. Despite decades of studies, expected theoretical performances of electronic devices based on 3C-SiC have never been demonstrated to date, mainly because of the poor 3C-SiC crystals quality. Even in the best free-standing 3C-SiC wafers, the extended defects (mainly stacking faults, SFs) density is still much higher than in the high quality commercial 4H or 6H-SiC wafers [2]. Consequently, most devices fabricated from this material have average performances [3]. A preliminary for the development of high performances 3C-SiC based devices is thus the availability of high quality bulk 3C-SiC crystals.

The need of a non-destructive tool to investigate both qualitatively and quantitatively the SFs in 3C-SiC crystals is hence of primary importance on the way of improving the crystalline quality of the materials. Recently, the power of diffuse X-ray scattering (DXS) has been demonstrated to quantitatively analyze SFs in thick 3C-SiC crystals [4]. Here we further develop this method and make use of it to characterize SFs in 3C-SiC crystals grown by Continuous Feed – Physical Vapor Transport (CF – PVT) coupled with Vapor – Liquid – Solid (VLS) heteroepitaxial growth. In this work particular emphasis is led on the versatility of the method which can be used, either on a qualitative level for routine analysis, a procedure made easy by the speed of the method (less than 20 minutes), or on a highly quantitative level in order to extract reliable values of SF densities.

2. Experimental

2.1 Crystal growth

3C-SiC crystals were deposited on two different substrates: a bare (0001) 4H-SiC substrate and a (0001) 6H-SiC covered with a ~1-2 μm thick (111) 3C-SiC buffer layer grown by VLS epitaxy We refer to the crystals grown on these substrates as (111)SiC and, (111)bSiC. Both samples exhibit a (111) out-of-plane orientation. The thickness of (111)SiC and (111)b SiC are 400 μm and 850 μm, respectively.

The CF-PVT process [5] combines high temperature chemical vapor deposition (CVD) for the in-situ formation of the polycrystalline SiC source, and physical vapor transport for the single crystal growth. Briefly, the crucible is divided in two regions (CVD region and sublimation region) by a porous graphite foam. The porous foam acts as a support for CVD SiC deposition and thus as a source for the sublimation step. The high purity polycrystalline SiC was fabricated from tetramethylsilane. The whole process has been described in details elsewhere [5, 6]. The growth took place at 1980°C with a growth rate of about 120 μm/h.

Concerning VLS epitaxy, starting from a 6H-SiC(0001) on-axis Si face seed, the initial 3C-SiC layer was grown in a Si-Ge melt. The deposition was carried out at atmospheric pressure in a home-made epitaxy apparatus equipped with a vertical cold wall reactor. Further details on the experimental set up have been given in Ref [7]. Briefly, the 6H-SiC seed was placed at the bottom of a graphite crucible. Si and Ge pieces were then stacked on top of the seed and heated under purified Ar up to 1500°C in order to form a liquid phase containing 25 at% Si. 3 sccm of propane was added when reaching the temperature plateau in order to start SiC growth by VLS mechanism.

For comparison purposes, we also analyzed a commercially available (001) 3C-SiC crystal

from HAST corporation.

2.2 X-ray diffraction

The crystals were characterized by high-resolution DXS. A laboratory diffractometer with a rotating Cu anode, a four-reflection monochromator and a curved position sensitive detector was used to record reciprocal space maps (RSMs). A five-movement sample holder allows precise sample positioning. The X-ray beam impinging on the sample is monochromatic (Cu $K\alpha_1$, $\Delta\lambda/\lambda=1.4\times10^{-4}$) and parallel in the detector plane ($\Delta\theta$=12 arcsec) with dimensions 10×0.09 mm² so that a large volume of the sample is analyzed which provides statistically significant averaged values. A detailed description of the set-up has been given elsewhere [8, 9, 10]. A RSM represents the scattered intensity in a particular (Q_x, Q_z) plane, where Q_x and Q_z are the components of the scattering vector **Q** ($Q = 4\pi \sin\theta / \lambda$) in the crystal plane and perpendicular to it, respectively. For (001) oriented 3C-SiC, RSMs are plotted in the ($Q_{[hk0]}$, $Q_{[00l]}$) plane, where $Q_{[hkl]}$ is the component of the scattering vector **Q** parallel to a given [*hkl*] direction. For (111) oriented 3C-SiC the RSMs are plotted in the ($Q_{[hkl]\perp}$, $Q_{[111]}$) plane, where $[hkl]_\perp$ is an in-plane direction perpendicular to [111].

3. Theoretical background

We shall start with the expression of the distribution of the diffracted intensity in the vicinity of a reciprocal lattice point (RLP) with reciprocal lattice vector h [11] :

$$I(\mathbf{q})=\int d\mathbf{r}\,\tilde{R}(\mathbf{r})\,V(\mathbf{r})\,G(\mathbf{r})\exp(i\mathbf{q}\mathbf{r})$$

where **r** is the correlation vector, *i.e.* the distance between two points in the crystal. **q** is the deviation of the scattering vector from the Bragg position (**q** = **Q** – **h**). $R(\mathbf{r})$ is the Fourier transform of the resolution function of the diffractometer. This term can be exactly evaluated [9] and will not be detailed here. $V(\mathbf{r})$ is correlation volume [11] which describes the effects of the shape and size of the coherently diffracting domains (mosaic domains), as well as their size fluctuations. $G(\mathbf{r})$ is the pair correlation function which describes the effects of lattice disorder and can be written:

$$G(\mathbf{r}) = \left\langle \exp\left\{ i\mathbf{h}\left[\mathbf{u}(\mathbf{r}) - \mathbf{u}(0)\right]\right\}\right\rangle \quad (1)$$

where $\mathbf{u}(\mathbf{r})$ is the displacement of the crystal lattice from its ideal position at point **r**. Assuming that the different defects don't interact (which can be reasonably assumed for low defect densities) then the displacement at point **r**, is simply the sum of all displacements due to different defects, $\mathbf{u}(\mathbf{r}) = \mathbf{u}_{SF}(\mathbf{r}) + \mathbf{u}_{\varepsilon}(\mathrm{r}) + \ldots$, where the subscript ε stands for 'heterogeneous strain' (this point is detailed below). If we further assume that the defects are statistically independent (*i.e.* the probability of finding a defect at point **r** is independent of the probability of finding another defect at point **r'**) then G(r) can be written:

$$G(\mathbf{r}) = G_{SF}(\mathbf{r}) \times G_{\epsilon}(\mathbf{r}) \times \ldots$$

Let us consider the term due to SFs. A stacking fault occurs when the regular stacking arrangement along the <111> direction, ABCABC, is violated, as in ABCA|C, for instance (the bar indicates the fault). The lattice displacement associated with such a fault is $\mathbf{u}_{AC} = (\mathbf{a}_h - \mathbf{b}_h)/3$, instead of $(-\mathbf{a}_h + \mathbf{b}_h)/3$ in the regular stacking arrangement [11]. In the previous equations we made use of the pseudo-hexagonal lattice parameters, $\mathbf{a}_h = (\mathbf{b} - \mathbf{a})/2$, $\mathbf{b}_h = (\mathbf{c} - \mathbf{b})/2$ and $\mathbf{c}_h = \mathbf{a} + \mathbf{b} + \mathbf{c}$. In the following we shall also make use of the pseudo-hexagonal indices, $H = (k - h)/2$, $K = (l - k)/2$ and $L = h + k + l$. The pair correlation function can hence be simply written in terms of the probabilities of finding an A (P_{AA}), B (P_{AB}) or C (P_{AC}) layer at

a distance r_{00L} from a starting A-layer:

$$G_{SF}(\mathbf{r}) = \left[P_{AA}(r_{00\mathrm{L}}) + P_{AB}(r_{00\mathrm{L}})\exp(i\Phi_{AB}) + P_{AC}(r_{00\mathrm{L}})\exp(i\Phi_{AC}) \right] \times \delta(\mathbf{Q} - \mathbf{h}_{\mathrm{HK0}}) \qquad (2)$$

where ϕ_{AB} and ϕ_{AC} are the phase shifts due to $\mathbf{u}_{AB}$ and $\mathbf{u}_{AC}$ when moving from A to B, or A to C layer [12] ($\phi_{AB} = -\phi_{AC} = -2\pi(H - K)/3$). The delta function in (2) shows that the intensity distribution is confined along the <00*L*> directions (*i.e.* the <*hhh*> directions) ; there is no intensity due to SFs in the {*HK*0} planes. This is simply a consequence of (1) which shows that when **u** is normal to **h**, the pair correlation function is equal to 1. In terms of *hkl*, this extinction condition can be stated as follows: for a fault lying in a (111) plane, those reflections with $h + k + l = 3\mathrm{N}$ (N being an integer) are unaffected. In a previous work [4] we made use of the difference-equation method [12] to derive the probabilities P_{ij}. These probabilities are simple functions of the stacking fault density (ρ_{SF}) and twin fault density. In the following we shall only consider ρ_{SF}.

Using the previous description, a schematic representation of a (00*l*) and a (*hhh*) RLP is displayed in figure 1. Figure 1a corresponds to a (00*l*) RLP of (001) oriented crystal. It exhibits streaks of diffuse scattering intensity along the different <111> directions because of faults lying in different {111} planes. There is an additional streak along [001] which is due to the truncation of the crystal lattice at the surface (the crystal truncation rod, CTR [13]). For the (111) oriented crystal, the (*hhh*) RLP (figure 1b) exhibits streaks along the <111> directions, excepted along [111] because of the above mentioned extinction condition. The small streak along [111] is the CTR. The data recorded in practice correspond to a partial projection of the RLP on the detection plane (the extent of this projection depends on the resolution perpendicular to detection plane). Therefore, features that are not contained in the detection plane may nonetheless appear. In both cases it can be seen that the measured RLP will exhibit a peculiar star-like pattern if the crystal contains SFs.

We now briefly discuss the $G_\varepsilon(\mathbf{r})$ and $V(\mathbf{r})$ terms. In addition to SFs, other defects may contribute to the diffracted intensity distribution. However, if these defects are not clearly identified, *i.e.* the $\mathbf{u}(\mathbf{r})$ can not be obtained, then it can be useful to describe the disorder in terms of the components of the homogeneous and heterogeneous strain tensor. A detailed expression of $G_\varepsilon(\mathbf{r})$ has been given elsewhere (see e.g. [11, 14]). In particular, the mosaicity σ gives rise to a broadening of the RLP in the direction perpendicular to $\mathbf{Q}$. Finally the shape of the mosaic domains influence the scattered intensity distribution, *via* the $V(\mathbf{r})$ term. In the present case, the mosaic domains were found to be very large (> 1μm) so that an accurate description of their shape is useless. We modeled the mosaic block size with cubes parallel to the surface, with a lognormal ditribution of their dimension, D. The corresponding expression of $V(\mathbf{r})$ can be found in [11].

4. Applications

In this section we use the previously detailed approach to analyze thick 3C-SiC crystals, starting with a well-characterized [15], commercially available, (001) crystal.

4.1. Commercial (001) 3C – SiC

The 3C-SiC crystals from HAST corporation are grown by CVD on undulant Si substrates, the ridges of the surface being parallel to the [1-10] direction. RSMs were recorded with the crystal oriented along [110] and [1-10] for both possible orientations of the crystal, *e.g.* upwards (the X-rays impinge on the free SiC surface) or downwards (the X-rays impinge on the SiC surface initially located at the SiC/Si interface), figure 2. All RSMs exhibit common features. The intense streak lying along the Ewald sphere and denoted PSD is due to the transmittance function of the PSD . Secondly, the streak parallel to the surface normal

(marked by a vertical arrow) is the CTR. In agreement with figure 1, the remaining streaks (marked by inclined arrows) can be attributed to SFs. The measured angle between the two remaining streaks and the surface normal is $\psi = 55°$ which indeed corresponds to the angle between the {111} planes and the crystal surface ($\psi_{(111),(001)} = 54.74°$).

Comparing figure 2a and 2c, it immediately appears that the streak intensity is higher along [1-10] than along [110], i.e. the SF density is weaker along [110]. This behavior has already been observed in these crystals [15] and is due to SF annihilation in the (-1-11) and (111) planes [15, 16]. Comparing figure 2a and 2b (or 2c and 2d) it is observed that an additional diffuse intensity appears around the Bragg peak for the downwards orientation. This can be attributed to a higher defect density at the highly mismatched SiC/Si interface as compared to the SiC surface [15]. It is interesting to notice that the streak intensity is equivalent along [1-10] and [110] for the downwards orientation (figure 2b and 2d), *i.e.* the SF density is isotropic at the interface. This can be easily understood considering that SF annihilation takes place during crystal growth.

In order to obtain quantitative information from the RSMs, we extracted and analyzed line scans, namely line scans along q_x (which are insensitive to faulting and allow to determine the mosaicity and mosaic domain size) and line scans along the <111> streaks (which allow to determine the SF density). The results are shown in figure 3. Let us first discuss the q_x-scans. The difference between the upwards and downwards orientation is striking: $D = 6$ µm and $\sigma = 0.012°$ for the upwards orientation and $D = 1.5$ µm and $\sigma = 0.02°$ for the downwards orientation. The presence of crystalline defects at the interface yields a mosaic structure with much smaller crystalline domains and a significantly increased mosaicity. Concerning SFs, we obtained $\rho_{SF} = 6.4\times10^3$ cm^{-1} along [1-10] and $\rho_{SF} = 1.4\times10^3$ cm^{-1} along [110], in excellent quantitative agreement with the values deduced from TEM for similar samples [15]. It must

be emphasized that the model nicely fits the data over almost 4 orders of magnitude with only 2 fitting parameters for the q_x-scans (D and σ) and 1 fitting parameter for the <111>-scans (ρ_{SF}). The excellent agreement with TEM observations validates the model which can be used reliably to analyze SFs in different 3C-SiC crystals.

4.2. (111) 3C-SiC

This crystal has been grown on 4H-SiC substrate. It is known that when cubic SiC is grown on a hexagonal polytype, two equiprobable epitaxial variants related to each other by a 60° rotation can occur. This comes from the two possible orientations of the trigonal (111) plane on the hexagonal (0001) plane. The boundary between the two variants is a special type of twin boundary known as double positioning boundary (DPB). For the present sample, optimized CF-PVT growth conditions allowed to select only one variant. However, we shall discuss this point further for the next sample. The RSM shown in figure 4a exhibit two diffuse streaks. The one with angle relative to the surface $\psi \approx 70°$ is due to SFs lying in the (-111) planes ($\psi_{(111),(-111)}$=70.53°), whereas the streak with angle $\psi \approx 55°$ is due to SFs lying in the (11-1) and (1-11) planes. According to figure 1 these streaks are not contained in the detection plane but they nonetheless appears because of the lack of resolution perpendicular to the detection plane . The same conclusions hold for figure 4b with SFs lying in the (11-1) plane on the one hand, and SFs lying in the (-111) and (1-11) planes on the other hand. We shall therefore only consider the [-111] and [11-1] streaks.

The simulation of the (111) q_x-scan is shown in figure 5a. The observed discontinuities in the central part of the peak are very likely due to large misoriented mosaic domains. Apart from the central part of the peak the model fits the data nicely over almost four orders of magnitude, especially in the profile tails, which allows to deduce a mosaic domain size of D = 6 μm. The mosaicity is found to be σ = 0.018°, although because of the deviations observed in

the central part of the peak, this latter parameter can not be used quantitatively and, hence, only serves as qualitative indicator of the crystalline quality. The fit of the <111> streaks is shown in figure 5b. It can be observed that the model perfectly fits the data over four orders of magnitude. The resulting SF density is $\rho_{SF} = 2.2\times10^4$ cm^{-1} in both directions, in excellent agreement with TEM observations.

We now turn to the second (111) SiC sample. Before CF-PVT growth the 6H-SiC substrate has been buffered with a 3C-SiC layer grown by VLS epitaxy. The XRD analysis of this buffer layer (not shown here) revealed that it is free of SFs or at least below the detection limit of our method, and that it exhibits both epitaxial variants, one variant being more abundant than the other. (Note that the VLS process has recently proven its ability to grow DPB free 3C-SiC layers [17]. Unfortunately, such sample has not been investigated by DXS yet.) This analysis allows to clarify the interpretation of the RSM figure. 4c. This RSM simply results from the superposition of two RSMs identical to those shown in figure 4a and 4b related to each other by a 60° rotation. The intensity of the second set of streaks (marked by dashed arrows and labeled DPB) is weaker as this epitaxial variant is less abundant than the other. (In figure 4d only one streak appears in the DPB set; this point is to date not clarified).

The simulation of the q_x-scan, figure 5c, yields a mosaic domain size D = 2.5 µm and a mosaicity σ = 0.015°. It appears that the presence of DPBs does not affect the mosaicity, but it clearly reduces the mosaic domain size. The simulation of the diffuse streaks provides a SF density $\rho_{SF} = 4\times10^4$ cm^{-1} which is significantly higher than for (111) SiC. These two latter features can be understood as follows: the DPB is an incoherent twin boundary whose energy is relaxed by the formation of SFs. Moreover, since coherence is lost from one epitaxial variant to the other, the overall mosaic domain size is reduced. Another important result is that SF are generated during CF-PVT growth (since the buffer was free of SFs) and that neither

the SFs nor the DPBs affect the mosaicity. This point will be the subject of further studies.

5. Conclusions

A method to study SFs in 3C-SiC crystal has been presented. This method is based on fast reciprocal space mapping and the simulation of the diffuse intensity streaks. Parameters of primary importance such as the SF density, the mosaic domain size and mosaicity can obtained. The method can be used qualitatively for routine analysis or quantitatively for in-depth studies of SFs in SiC.

References

[1] A. Fissel, Phys. Rep. **379**, 149 (2003).

[2] H. Nagasawa, K. Yagi, T. Kawahara, N. Hatta, G. Pensl, W. J. Choyke, T. Yamada, K. M. Itoh, and A. Schoner, in *Silicon Carbide*, edited by W.J. Choyke, H. Matsunami, and G. Pensl (Springer, New-York, 2004), pp. 207.

[3] A. Schöner, M. Bakowski, P. Ericsson, H. Strömberg, H. Nagasawa, and M. Abe, Mater. Sci. Forum **483-485**, 801 (2005).

[4] A. Boulle, D. Chaussende, L. Latu-Romain, F. Conchon, O. Masson, R. Guinebretière, Appl. Phys. Lett. 89, 091902 1-6 (2006).

[5] D. Chaussende, L. Latu-Romain, L. Auvray, M. Ucar, M. Pons, and R. Madar, Mater. Sci. Forum 483-485, 225 (2005).

[6] D. Chaussende, M. Ucar, L. Auvray, F. Baillet, M. Pons, and R. Madar, Crystal Growth & Design 5, 1539 (2005).

[7] M. Soueidan and G. Ferro, Adv. Funct. Mater. 2006, 16, 975-979.

[8] A. Boulle, O. Masson, R. Guinebretière, A. Dauger, Appl. Surf. Sci. 180, 322-327 (2001).

[9] A. Boulle, O. Masson, R. Guinebretière, A. Lecomte, A. Dauger, J. Appl. Crystallogr. 35, 606-614 (2002).

[10] O. Masson, A. Boulle, R. Guinebretière, A. Lecomte, A. Dauger, Rev. Sci. Instr. 76, 063912 1-7 (2005).

[11] A. Boulle, F. Conchon, R. Guinebretière, Acta Crystallogr.A 62, 11-20 (2005).

[12] B. E. Warren, *X-ray diffraction*. (Addison-Wesley, New-York, 1969).

[13] I. K. Robinson, Phys. Rev. B **33** (6), 3830 (1986).

[14] A. Boulle, R. Guinebretière, A. Dauger, J. Phys. D: Appl. Phys. 38, 3907-3920 (2005).

[15] E. Polychroniadis, M. Syvajarvi, R. Yakimova, and J. Stoemenos, J. Cryst. Growth **263** (1-4), 68 (2004).

[16] H. Nagasawa, K. Yagi, and T. Kawahara, J. Cryst. Growth 237-239, 1244 (2002).

[17] M. Soueidan, G. Ferro, B. Nsouli, M. Roumie, E. Polychroniadis, M. Kazan, S. Juillaguet, D. Chaussende, N. Habka, J. Stoemenos, J. Camassel, Y. Monteil, Crystal Growth & Design 6, 2598 (2006).

Figure caption

Figure 1: schematic representation of an (00*l*) RLP of an (001) oriented crystal (a), and of an (*hhh*) RLP of a (111) oriented crystal (b). In both cases, streaks of diffusely scattered intensity extend along the <111> directions, except for (b) where the [111] streak is extinguished.

Figure 2: RSMs of the (002) RLP of (001) oriented 3C-SiC: (a) upwards along [110], (b) downwards along [110], (c) upwards along [1-10], (d) downwards along [1-10].

Figure 3: (a) q_x-scans performed through the centre of the (002) RLP for the upwards orientation (lower curve) and the downwards orientation (upper curve). (b) line scans performed along [111] (lower curve) and [1-11] (upper curve). Notice that the logarithm of the intensity is plotted and that the curves are shifted vertically for clarity (grey dots: experimental; line: simulation).

Figure 4: RSMs of the (111) RLP of (111) oriented 3C-SiC crystals: (a) along [2-1-1] for the first crystal, (b) along [11-2] for the first crystal, (c) along [2-1-1] for the second crystal, (d) along [11-2] for the second crystal.

Figure 5: (a) q_x-scan performed through the centre of the (111) RLP of the first crystal. (b) line scans performed along [-111] (lower curve) and [11-1] (upper curve) for the first crystal. (c) q_x-scan performed through the centre of the (111) RLP of the second crystal. (d) line scans performed along [-111] (lower curve) and [11-1] (upper curve) for the second crystal. Notice

that the logarithm of the intensity is plotted and that the curves are shifted vertically for clarity (grey dots: experimental; line: simulation).

Figure 1

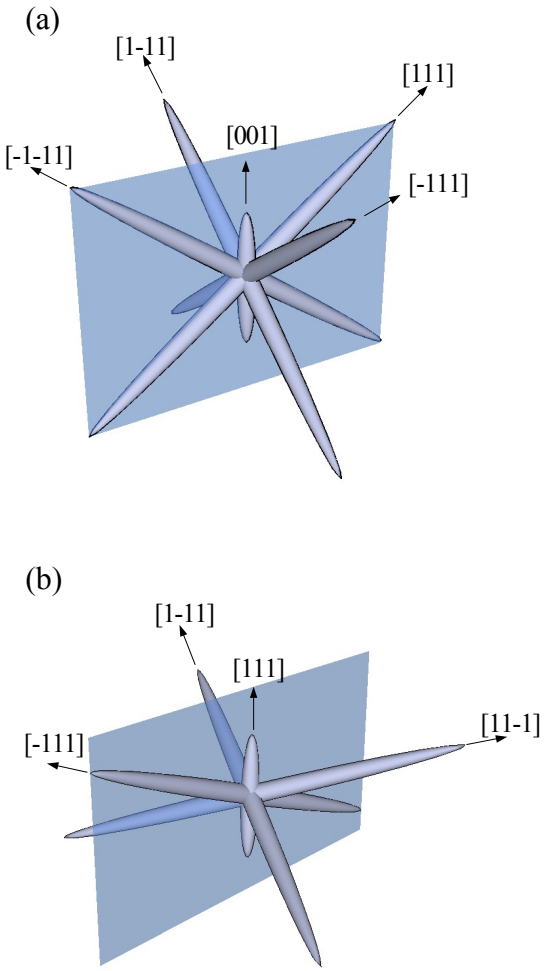

Figure 2

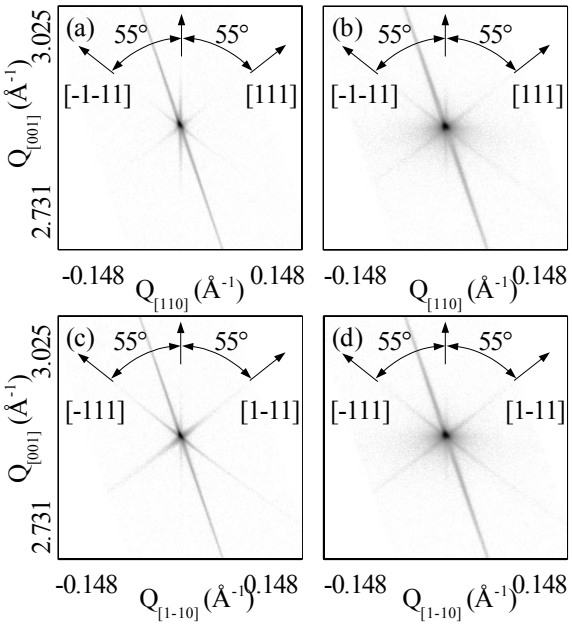
(a)
55°
55°
[-1-11]
[111]
(b)
55°
55°
[-1-11]
[111]
3.025
$Q_{[001]}$ (Å^{-1})
2.731
-0.148
$Q_{[110]}$ (Å^{-1})
0.148
-0.148
$Q_{[110]}$ (Å^{-1})
0.148
(c)
55°
55°
[-111]
[1-11]
(d)
55°
55°
[-111]
[1-11]
3.025
$Q_{[001]}$ (Å^{-1})
2.731
-0.148
$Q_{[1-10]}$ (Å^{-1})
0.148
-0.148
$Q_{[1-10]}$ (Å^{-1})
0.148

Figure 3

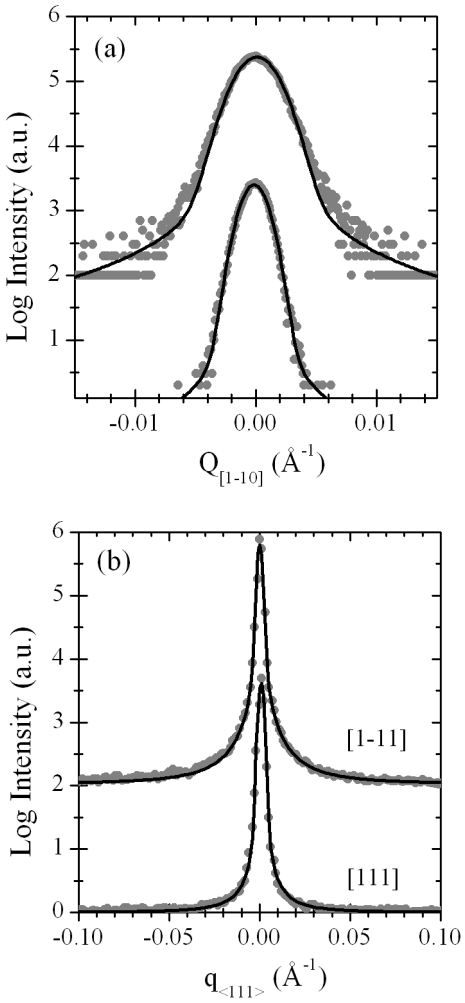
(a)
Log Intensity (a.u.)
6
5
4
3
2
1
-0.01
0.00
0.01
Q[1-10] (Å-1)
(b)
Log Intensity (a.u.)
[1-11]
[111]
6
5
4
3
2
1
0
-0.10
-0.05
0.00
0.05
0.10
q<111> (Å-1)

Figure 4

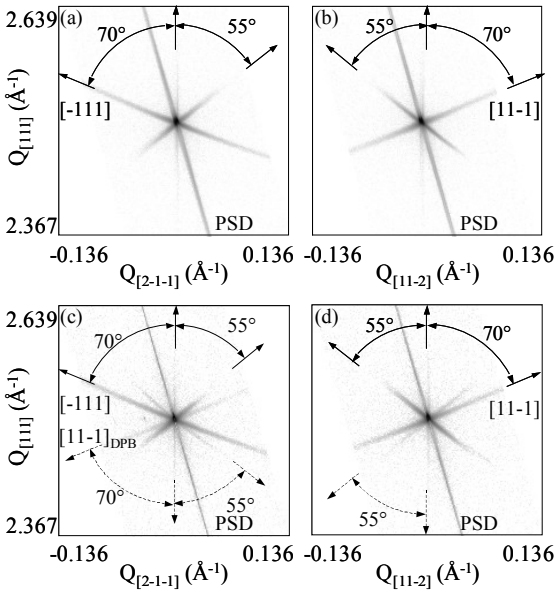
(a)
70°
55°
[-111]
PSD
2.639
2.367
$Q_{[111]}$ (Å^{-1})
-0.136
0.136
$Q_{[2-1-1]}$ (Å^{-1})
(b)
55°
70°
[11-1]
PSD
-0.136
0.136
$Q_{[11-2]}$ (Å^{-1})
(c)
70°
55°
[-111]
[11-1]$_{DPB}$
70°
55°
PSD
2.639
2.367
$Q_{[111]}$ (Å^{-1})
-0.136
0.136
$Q_{[2-1-1]}$ (Å^{-1})
(d)
55°
70°
[11-1]
55°
PSD
-0.136
0.136
$Q_{[11-2]}$ (Å^{-1})

Figure 5

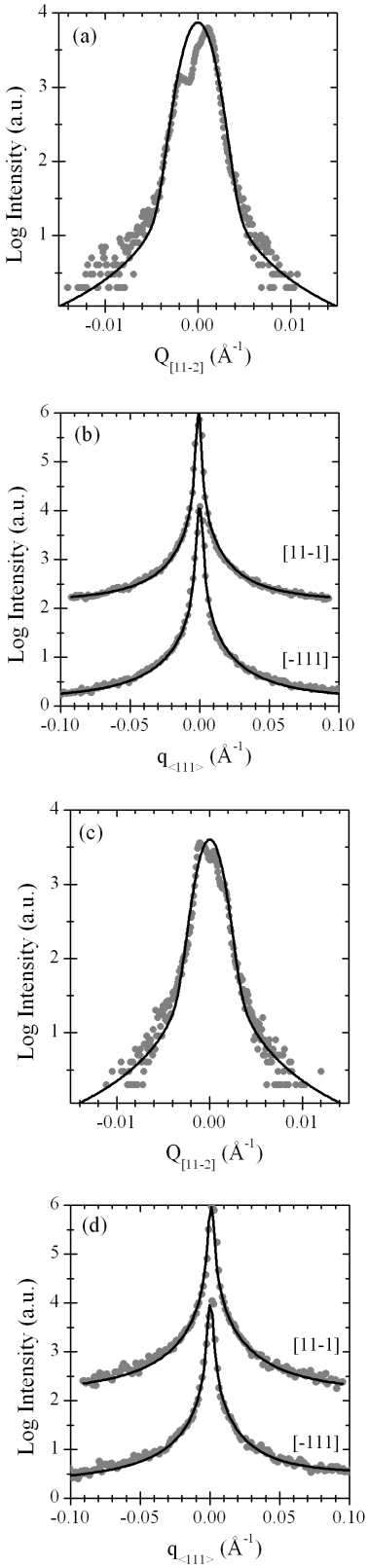
(a)
Log Intensity (a.u.)
$Q_{[11-2]}$ (Å^{-1})
(b)
[11-1]
[-111]
Log Intensity (a.u.)
$q_{<111>}$ (Å^{-1})
(c)
Log Intensity (a.u.)
$Q_{[11-2]}$ (Å^{-1})
(d)
[11-1]
[-111]
Log Intensity (a.u.)
$q_{<111>}$ (Å^{-1})